

## Simulating the RFOFO Cooling Ring with GEANT

Amit Klier, Gail G. Hanson  
University of California, Riverside  
Email: [Amit.Klier@ucr.edu](mailto:Amit.Klier@ucr.edu)

October 2004

### *Abstract*

A simulation of the RFOFO cooling ring was performed using GEANT. This note describes the simulation software, ring geometry, and how the magnetic fields, RF acceleration and absorbers were simulated. It also describes the ring performance and how the parameters were set, first by running with only the magnetic field on, then using “ideal” absorbers (no scattering or straggling). Finally an actual cooling test with “realistic” absorbers is given.

## 1. Introduction

The RFOFO cooling ring was proposed in [1] as a way of cooling muon beams both transversely and longitudinally (6-D cooling). The basic ring consists of 12 identical sections, each containing two tilted solenoids, six RF cavities and a wedge absorber filled with liquid hydrogen. The focusing lattice is similar to the FOFO lattice, but with unequal distances between the solenoids and beam bending, the result of the vertical component of the magnetic field due to the solenoid tilt.

Simulations of the RFOFO ring with ICOOL [1],[2] have shown good 6-D cooling performance, compared to other existing cooling ring designs. Another simulation [3] was in good agreement with the ICOOL simulation results.

## 2. Basics

### *2.1 Simulation software*

The simulation software, MUC\_GEANT [4], is an application of GEANT 3.21 [5] specially designed for muon cooling simulation. The Runge-Kutta routine was changed to include electric fields, so that RF acceleration would be simulated properly. The software is also data-driven, i.e. it allows the user to change the cooling channel parameters, such as geometry, RF frequency/gradient and physics processes, without changing the code.

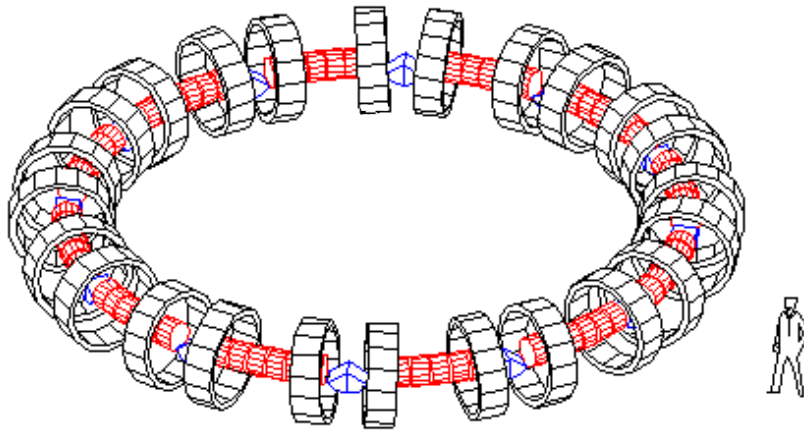


**Figure 1: A three-dimensional view of the RFOFO ring (a GEANT drawing).**

## 2.2 Geometry

A GEANT drawing of the RFOFO ring is shown in Figure 1. The geometry used here is as in [1],[2],[3]. The ring is made up of 12 identical cells. Each cell has an arc length of 2.75 meters along the ring's central line (which defines the reference  $z$  axis). The ring cell starts at the center of the absorber, which is a wedge of  $110^\circ$  opening angle pointing upwards. The wedge is 40 cm in radius and width, and its tip is 9.5 cm above the central line. In this simulation, the absorbers have no windows.<sup>1</sup> Next are six RF cavities, shown as cylinders, 28.75 cm long and 25 cm in radius of aperture, centered between  $z=55$  and 220 cm, 33 cm apart on the central line.

The two solenoids are 50 cm long and have an inner radius of 77 cm and an outer radius of 88 cm. One solenoid is centered at  $z=55$  cm and tilted by  $+3^\circ$  with respect to the horizontal plane. The second solenoid is centered at  $z=220$  cm and tilted by  $-3^\circ$ . Both solenoids are centered 10 cm "outside" the ring central line, in such a way that the circular trajectory along the central line follows more or less the magnetic field lines. The solenoids are shown here only for display purposes, since the magnetic field is read in from an external file (see following subsection). A single cell is shown in Figure 2.

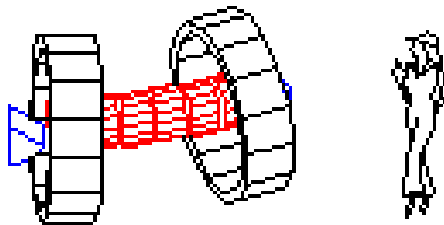


**Figure 2: A single cell of the RFOFO ring. Note that only the acceptance of the RF cavities is shown here (in red), whereas actual cavities would have a much larger volume.**

<sup>1</sup> The fact that the liquid-hydrogen-filled absorbers have no windows makes them unrealistic. However, the term "realistic absorber" is used here to describe the simulation of physics processes in the material.

### 2.3 The magnetic field simulation

The magnetic field in the ring is calculated using an external code [6] to generate a field map with a spacing of 1 cm in each direction. The field map is written into a data file that the simulation software uses to determine the magnetic field at each point along a particle's trajectory.

### 2.4 RF cavity simulation

A simplified model is used to simulate the electric field in the RF cavities. The field is purely axial in the cavity reference frame, where the  $z$  axis is tangential to the ring central line, at the center of the cavity. The electric field in the cavity frame is given by:

$$E_x = 0, \quad E_y = 0 \quad \text{and} \quad E_z = G \sin(2\pi f t + \varphi_i + \varphi_0), \quad (1)$$

where  $G$  is the RF gradient,  $f$  is the frequency,  $\varphi_i$  is the relative phase of the  $i^{\text{th}}$  cavity, determined by the entry time of the "reference particle" in each of the 72 cavities, and  $\varphi_0$  is the global phase offset, common to all cavities in the ring. The RF frequency must be an integer number times the reference particle revolution frequency, and also close to 201.25 MHz, which is the design frequency. Details of the parameter determination and the choice of the reference particle are given in section 3.2.

The gradient and the global phase offset are then optimized in order to achieve the best acceptance for a beam in the ring. Details are given in section 4.2.

## 3. Running with Only Magnetic Field On

In the first test of the ring simulation only the magnetic field was turned on. Some of the basic features of the lattice, such as closed orbits and dispersion functions, were studied. A reference particle, used to determine each cavity's relative phase, was also chosen from the closed orbits that were found.

### 3.1 Closed orbits and the dispersion function

Muons were "injected" at the boundary of the cell, in the middle of the absorber, which is one of the two planes in a cell where the transverse momentum vanishes for a closed orbit. For each initial (longitudinal) momentum, a unique closed orbit was determined by scanning the plane, and finding the point to which the muon returns every time it crosses the measuring plane at middle of the absorber. Some of the closed orbits are shown in Figure 3 (compare to Fig. 5 in [3] and Fig. 5(a) in [2]).

Dispersion functions in  $x$  and  $y$  at the absorber central plane (and approximately the absorber as a whole) can be derived from these closed orbits, as shown in Figure 4 (compare to Fig. 7 in [3] and Fig. 5(b) in [2]). One can see the linear dependence of the  $y$  (vertical) offset on the energy in Figure 4, which means that a wedge absorber should point upwards.

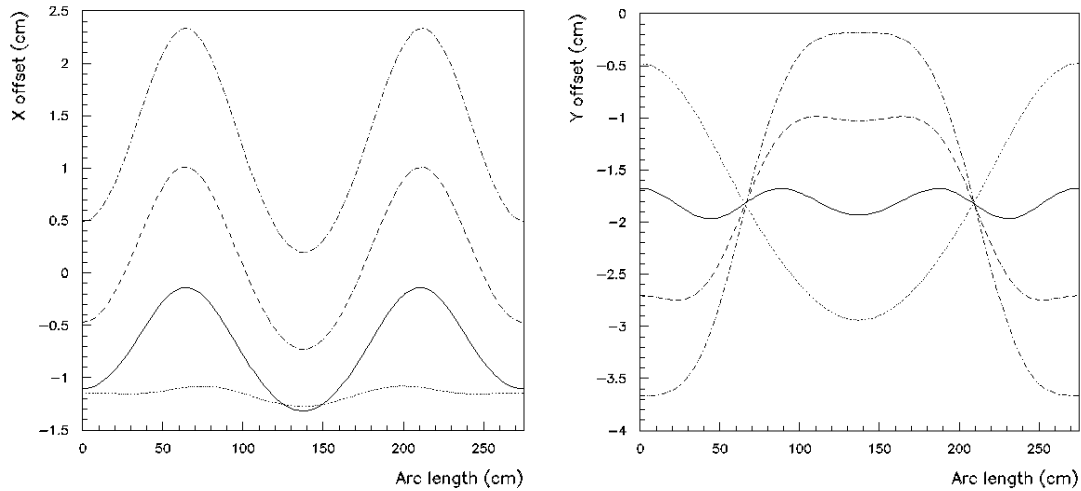


**Figure 3: Closed orbits in a cell – deviation from the ring’s central line, in radial direction (left plot) and vertical direction (right plot). The different line types represent different energies: solid – 227 MeV (“reference particle” with  $p = 201$  MeV/c), dotted, dashed and dot-dashed show 200, 250 and 270 MeV muons, respectively.**

### 3.2 The reference particle (clock)

The reference particle is a muon that runs in a closed orbit and is used as a “clock” to determine the RF frequency and set the entry times for each cavity in the ring. The clock should satisfy the following conditions:

- Its turn period must be an integer multiple of  $1/(201.25 \text{ MHz})$ ;
- The muon’s momentum should be around 200 MeV/c.

The closed-orbit muon that was chosen as the reference particle has a momentum of 200.96 MeV/c. With a turn period of 124.22 ns, its 25<sup>th</sup> harmonic is 201.26 MHz. This is as close to the required value as could be achieved within the resolution in GEANT.

The solid lines in Figure 3 show the reference particle’s coordinates relative to the ring’s central line.

## 4. Simulations with an Ideal Absorber

The next step in the simulation was to turn on the RF cavities and absorbers and test the ring’s behavior under “ideal” conditions, i.e. no multiple scattering or straggling in the absorber material. In this case, the cooling is expected to be optimal, and the ring stability can be studied at various RF voltages and phase offsets to find the best acceptance.

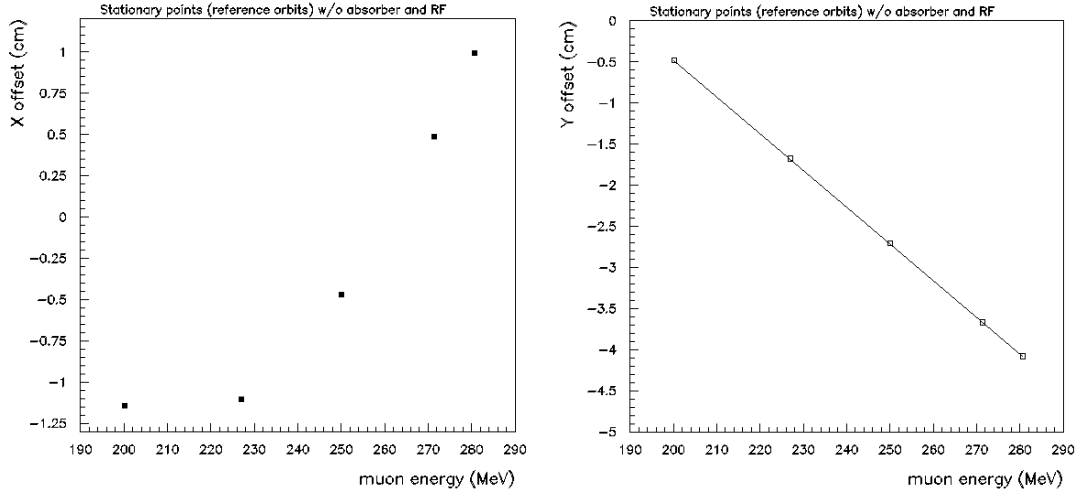


**Figure 4: Points of intersection of the closed orbits and the measuring plane at the center of the absorber, forming the dispersion functions, in the radial direction (left plot) and vertical direction with linear fit (right plot).**

#### 4.1 The performance of an “ideal” ring

The performance of the ring was tested with single muons injected at various starting points in phase space, corresponding to the central,  $\pm 1\sigma$  and  $\pm 2\sigma$  values of the Gaussian distributions in  $x$ ,  $y$ ,  $t$ ,  $p_x$ ,  $p_y$  and  $E$  following the beam specification from [3]:

- $\sigma_x = \sigma_y = 4.25$  cm (central values at the reference orbit crossing – see Figure 4);
- $\sigma_{p_x} = \sigma_{p_y} = 30$  MeV/c (central value = 0);
- $\sigma_{ct} = 8$  cm (central arrival time is defined as  $t = 0$ );
- $\sigma_{AE} = 20$  MeV (central  $E = 227$  MeV – the reference particle’s total energy).

Note that the “central values” are only approximations, since the symmetry of the ring is broken with the introduction of absorbers and acceleration, and the reference orbit is not the same as it was without RF and absorbers. The new reference orbit, referred to as the “equilibrium orbit”, is discussed below.

The cooling performance over 30 “ideal” ring turns is demonstrated in Figure 5, where the evolution of  $y$  is shown for various initial muon energies. Unlike Figure 3, the lines here do not show the whole track, and the points were sampled only at the cell boundary plane (at the middle of the wedge) – a total of 12 samples in each ring turn.

Figure 6 shows all the 36 projections of the six phase-space dimensions (different rows) when varying each of them (different columns). The bands show the  $\pm 1\sigma$  regions in each dimension. As seen in the figure, all the lines converge at a single point in phase space, which defines the “equilibrium orbit”. The equilibrium orbit is very close (but not identical) to the reference orbit. It has a very small transverse momentum ( $\sim 1.3$  MeV) at the starting point (the reference orbit has no initial transverse momentum), its  $p_z$  is 0.3 MeV higher and the starting coordinates are 0.1 mm away from their “original” position.

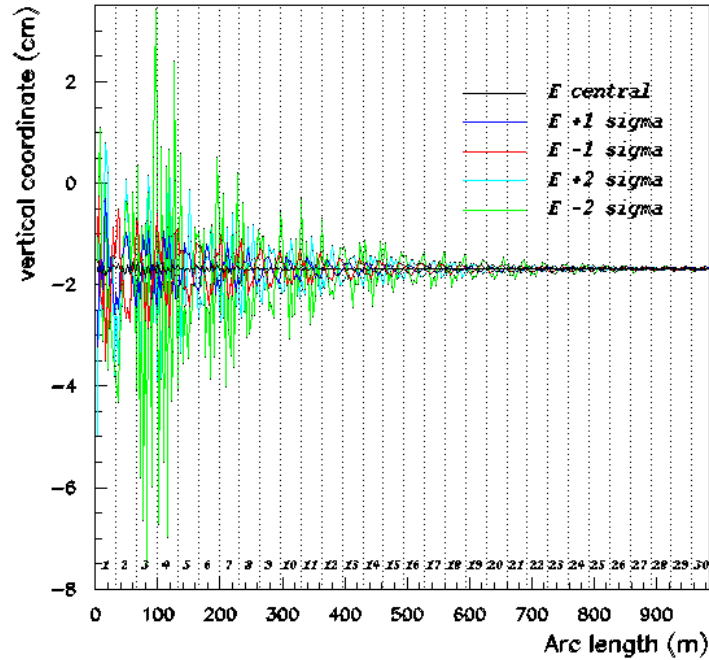


Figure 5: Running with an ideal absorber: the evolution of  $y$  for five different initial energies in 30 ring turns (each turn is marked by a dotted line and a number at the bottom of the plot). The transverse coordinates, momentum and entry time were all set to the central value. The black line shows initial energy at the central value, the dark-color lines indicate  $\pm 1\sigma$  in energy and the light-color lines indicate  $\pm 2\sigma$  values. All the lines eventually converge around  $-1.68$  cm in  $y$ .

A few observations from Figure 6:

- 1) The canonical pairs  $x-p_x$ ,  $y-p_y$  and  $t-E$  – behave similarly for the same initial conditions.
- 2) Large variations ( $\pm 2\sigma$ ) in the transverse directions are reflected in longitudinal directions, whereas small variations ( $\pm 1\sigma$ ) have much weaker coupling.
- 3) Time variation almost doesn't affect transverse directions, whereas the energy variation relates to the transverse coordinates through the dispersion function.
- 4) In general, varying  $p_x$ ,  $p_y$  or  $E$  influences the fluctuations in all 6 coordinates more than varying  $x$ ,  $y$  or  $t$  by the same number of standard deviations ( $\sigma$ 's). This means that the initial beam ellipses are a bit elongated (not taking into account correlations) in the direction of the momentum/energy.
- 5) The transverse coordinates and momenta show a “beating” pattern, where the horizontal and vertical degrees of freedom are exchanged back and forth, with a period of  $\sim 7$  turns.

The RF gradient in this demonstration was set to 13.5 MV/m, which is similar to the values used in [1],[3]. The phase offset was set to  $\varphi_0 = -12.6^\circ$ , which is the “equilibrium phase”, i.e. the value of the equilibrium orbit (a different  $\varphi_0$  would result in an offset in  $t$  projection as the “beam” converges).

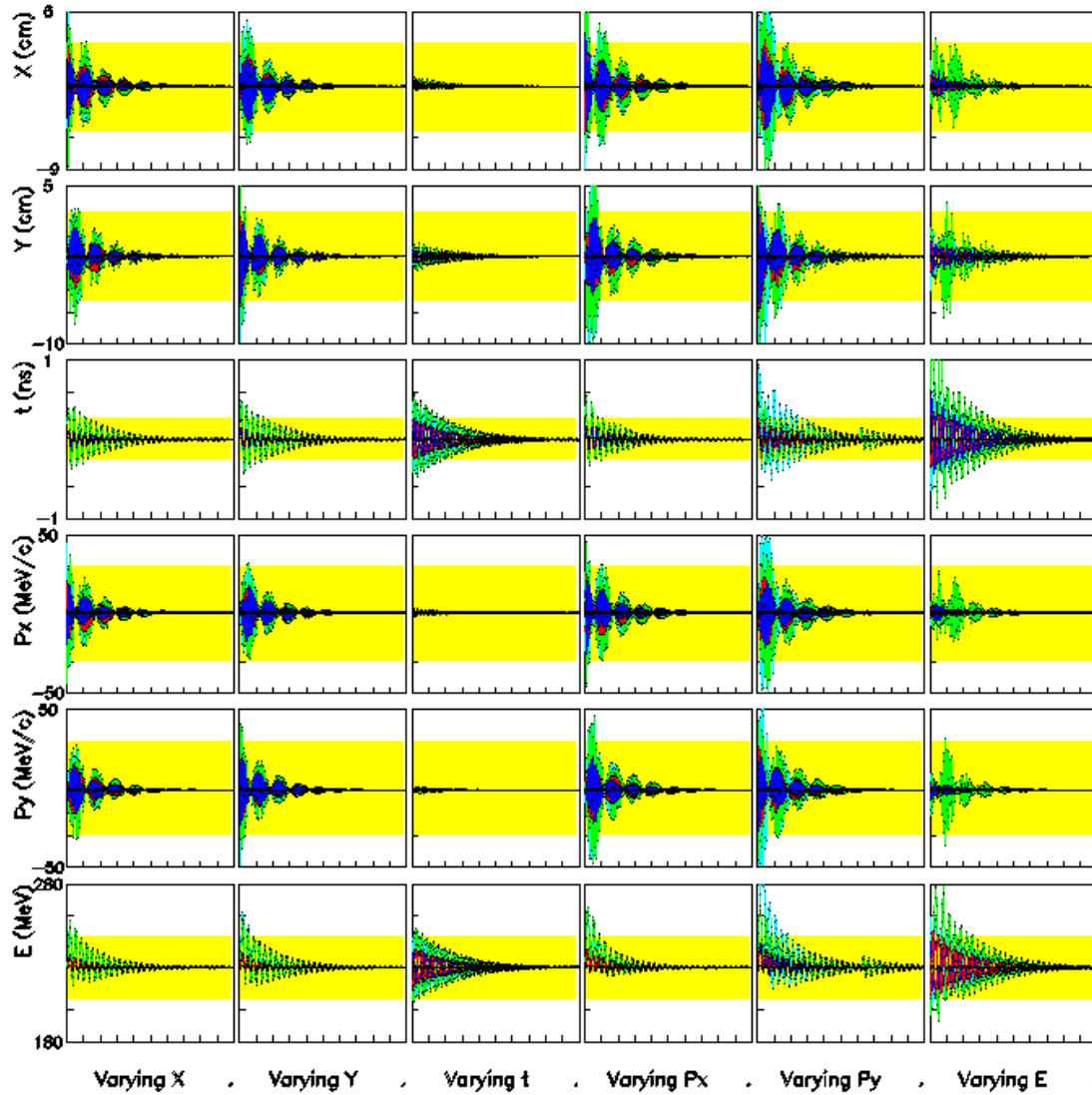
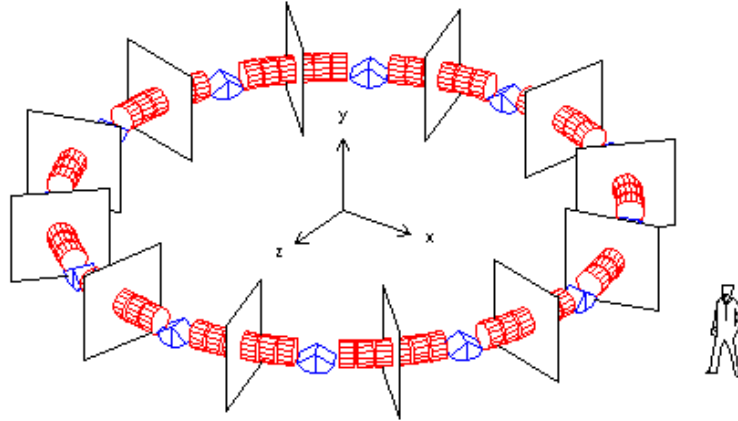


Figure 6: All six phase-space projections, varying (separately) each of the 6 phase-space coordinates by  $\pm 1\sigma$  and  $\pm 2\sigma$  around the central value. The same number of turns (30) and color-coding as in Figure 5 are used here. In addition, the light-shaded bands indicate the  $\pm 1\sigma$  regions in each of the projected coordinates.

## 5. Cooling a Muon Beam with “Realistic” Absorbers

In this section, all the physical processes, in particular multiple scattering and straggling, were turned on. The random nature of these processes requires large statistics samples, i.e. “beams,” to demonstrate the ring cooling performance.



**Figure 7: Location of the virtual detectors used to measure the beam in the simulated RFOFO ring. The solenoids are not shown here.**

### 5.1 The Beam

The beam that was employed is the same one that was used in [2],[3], where it is also described. The GEANT simulation software was modified to be fully compatible with the ICOOL input format (the beam itself) and its output format (for emittance calculation). This modification will make the change from ICOOL to GEANT simulation easier for future cooling channel designs as well.

The input file contains initial coordinates and momenta of 2,000 muons. However, for the simulation described here only partial samples (up to 1,000 particles) were used.

### 5.2 Beam measurement

The momenta and transverse coordinates of the muons in the beam are “measured” using virtual detector planes located in the middle of each cell, between the 3<sup>rd</sup> and 4<sup>th</sup> RF cavities, as seen in Figure 7. The output is written into an ICOOL format output file that can be read by ecalc9 emittance calculation software [7].

### 5.3 Ring optimization: finding the ideal working point

The last step before the actual simulation was to find the region of highest acceptance of the muon beam. The two remaining free parameters of Equation (1), the gradient  $G$  and the global phase offset  $\varphi_0$ , were scanned in order to find the optimal working conditions.

“Best acceptance” is achieved at the point in  $G$ - $\varphi_0$  space where transmission of a 400-muon beam after six turns<sup>2</sup> is maximal, with muon decay turned off. Figure 8(a-d) show the transmissions as function of  $\varphi_0$  for four values of  $G$ . The maximal survival rate from parabolic fits and the phase  $\varphi_0$  where it occurs, as functions of the gradient  $G$ , are shown in Figure 8(e) and (f), respectively.

<sup>2</sup> Six turns were chosen since most fluctuations that did not cause instability (muon escape) are suppressed by then, cf. Figure 6 (where 6 turns correspond to 2 horizontal tick marks).

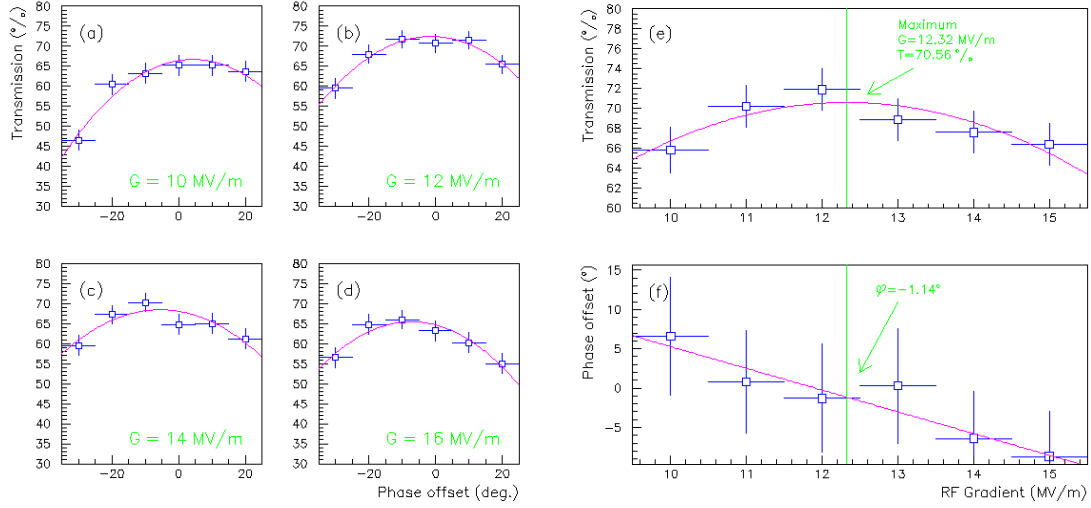


**Figure 8:** (a-d) The survival rate (as defined in the text), in percents, as a function of the phase offset ( $\varphi_0$ ) for 4 values  $G$  between 10 and 16 MV/m, shown with parabolic fits (curves). (e) The maximal survival rates from the parabolic fits (fitted to a parabola as well) and (f) the phase offset where they occur (with a linear fit), as functions of the gradient. The errors shown are from beam statistics.

The working point was chosen as the maximum of the fitted parabola in Figure 8(e). The values are  $G = 12.32$  MV/m, and  $\varphi_0 = -1.14^\circ$ . The change in the phase  $\varphi_0$  when decreasing the survival rate by 1% from the maximum in the fit is around  $\pm 10^\circ$  (between  $9^\circ$  and  $11^\circ$ , depending on  $G$ ). The sensitivity of the gradient is  $\pm 2$  MV/m.

#### 5.4 Cooling performance and comparison with other simulations

A beam of 1000 muons was used to demonstrate the cooling performance of the ring. At first, muon decay was turned off, to study beam dynamics and losses not from decay. Figure 9 shows the 2-dimensional distributions for the three canonical-conjugate pairs ( $x$ - $p_x$ ,  $y$ - $p_y$  and  $E$ - $t$ ) in 4 “stations” – at the starting point (the initial beam), and after 5, 10 and 15 turns. The reduction in phase-space volume is visible in every dimension.

Finally, muon decay was turned on for the same 1000-muon beam. A comparison of the beam transmission with and without muon decay is shown in Figure 10.

The emittance was calculated using ecalc9 [7], which is the standard tool for this purpose. A comparison of the GEANT simulation performance with that of ICOOL [2], for transverse, longitudinal and 6-D emittance is shown in Figure 11(a-c), respectively. Figure 11(d) shows the merit factor, defined as  $M = (\varepsilon_{6D}^{\text{initial}} / \varepsilon_{6D}^{\text{final}}) \cdot T$ , where  $\varepsilon_{6D}^{\text{initial}}$  and  $\varepsilon_{6D}^{\text{final}}$  are the initial and final 6-dimensional emittance, respectively, and  $T$  is the beam transmission. The merit factor of the RFOFO ring after 15 turns is around 100.

A comparison of beam transmission and merit factor after 10 turns for GEANT and the other two RFOFO ring simulations [2],[3] is shown in Table 1, where they all seem to agree well.

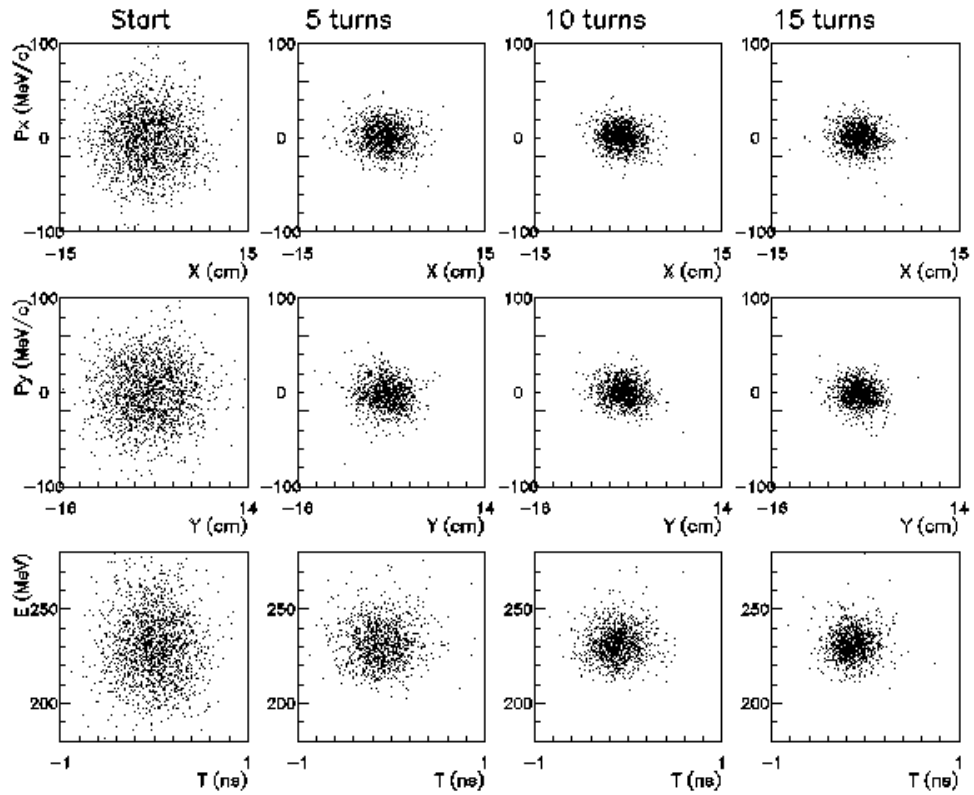


Figure 9: The distributions of  $p_x$  vs.  $x$  (upper row),  $p_y$  vs.  $y$  (middle row) and  $t$  vs.  $E$  (lower row) in four “stations” along the beam path: initial beam (left column), after 5 ring turns (second-to-the-left column), after 10 turns (second-right column) and 15 turns (right column).

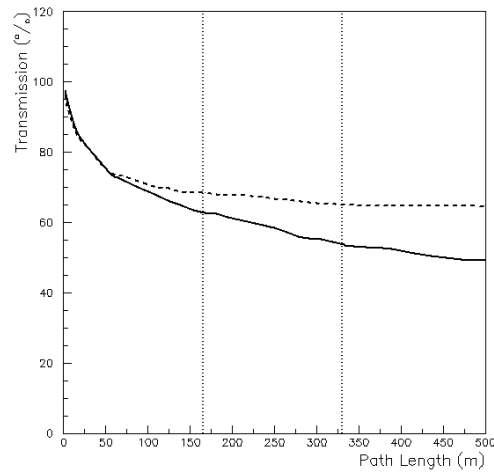
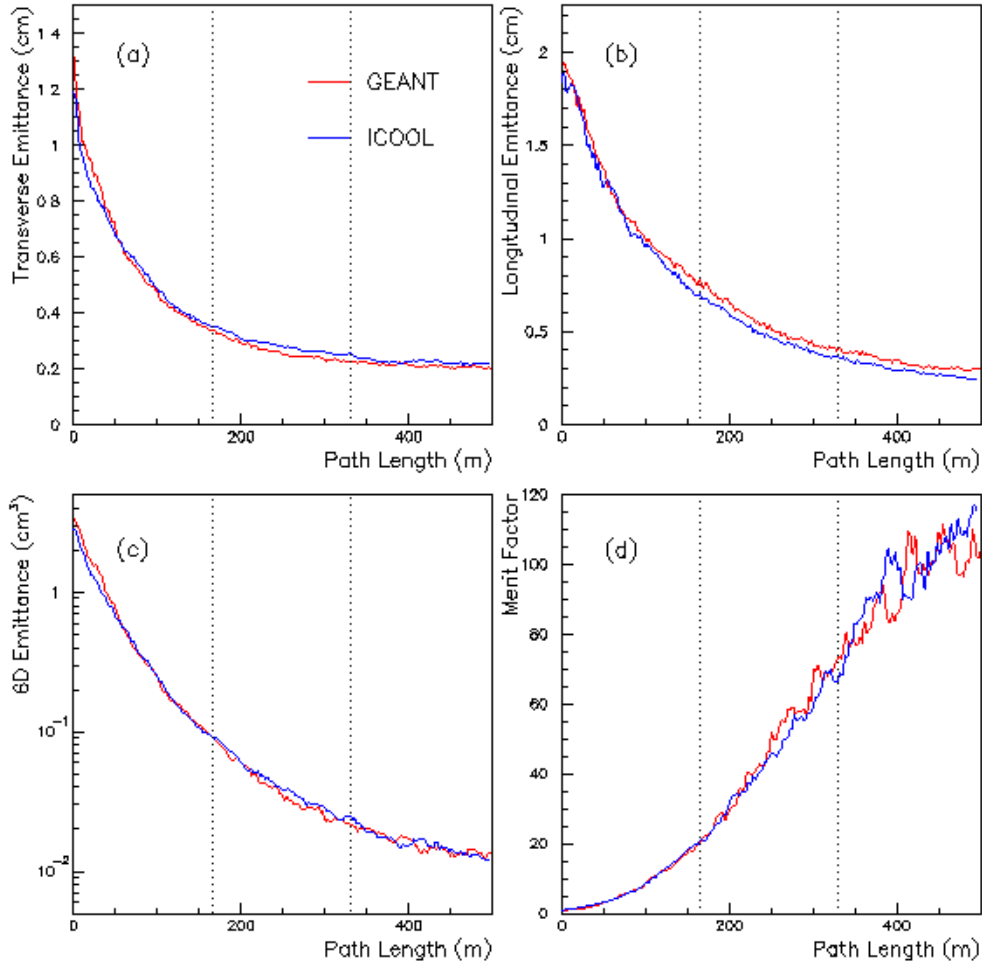


Figure 10: Beam transmission with and without muon decay (solid and dashed lines, respectively) for 15 ring turns. The dotted lines mark 5 and 10 ring turns.



**Figure 11: A comparison between GEANT (red line) and ICOOL (blue) for transverse emittance (a), longitudinal emittance (b), 6-dimensional emittance (c) and merit factor (d) in 15 ring turns. The dotted lines mark 5 and 10 turns.**

## 6. Summary and Outlook

A simulation of the RFOFO ring was performed using GEANT. The results agree well with other simulations that were performed in the past. The software package was modified, and is now more flexible, and can handle “standard” ICOOL input and output, that can be used in existing emittance calculation tools.

More software changes are still required in order for the GEANT muon cooling simulation package to be fully compatible with different geometries that may include asymmetric rings (e.g. with injection cells) and any desired geometry, including gas-filled rings and other cooling channels. In addition, new methods for simulating RF cavities, similar to the magnetic field maps, are planned.

**Table 1: Beam transmission with and without decay and merit factor after 10 turns for various RFOFO simulations.**

Simulation software	Trans. no decay	Trans. with decay	Merit factor
ICOOL [2]	n/a	58%	66
MC-264 [3]	70%	56%	55
GEANT	72%	57%	70

## Acknowledgements

The authors wish to thank Rajendran Raja of Fermilab, Bob Palmer, Rick Fernow and Steve Kahn of Brookhaven, and Romulus Godang of Mississippi.

## References

- [1] J.S. Berg, R.C. Fernow, R.B. Palmer, “An Alternating Solenoid Focused Ionization Cooling Ring”, MC-Note 239, March 2002.
- [2] R.C. Fernow, J.S. Berg, J.C. Gallardo, R.B. Palmer, “Muon Cooling in the RFOFO ring”, MC-Note 273, April 2003;  
R.C. Fernow, private communication.
- [3] V. Balbekov, “Simulation of RFOFO Ring Cooler with Tilted Solenoids”, MC-Note 264, November 2002.
- [4] R. Raja, “MUC\_GEANT – Data Driven GEANT for Ring Coolers”, July 2002.  
[http://www.fnal.gov/projects/muon\\_collider/eexchange/Muc\\_GEANT/muc\\_GEANT\\_doc.htm](http://www.fnal.gov/projects/muon_collider/eexchange/Muc_GEANT/muc_GEANT_doc.htm)
- [5] “GEANT – Detector Simulation and Simulation Tool”, CERN Program Library Long Write-up W5013, March 1994.  
[http://wwwasdoc.web.cern.ch/wwwasdoc/GEANT\\_html3/GEANTall.html](http://wwwasdoc.web.cern.ch/wwwasdoc/GEANT_html3/GEANTall.html)
- [6] S. Bracker, ”Magnetic Field Maps for the RFOFO Muon Cooling Ring”, MC-Note 271, March 2003.
- [7] G. Penn, ecalc9 code.  
<http://ist-socrates.berkeley.edu/~gpenn/Muon/ecalc9v2.for>